Euclidean bridge to the relativistic constituent quark model

T. J. Hobbs, Mary Alberg, and Gerald A. Miller

Phys. Rev. C **95**, 035205 — Published 20 March 2017

DOI: 10.1103/PhysRevC.95.035205

NT@UW-16-08

A Euclidean bridge to the relativistic constituent quark model

T. J. Hobbs[1*] and Mary Alberg[1,2], Gerald A. Miller[1]

[1] *Department of Physics, University of Washington, Seattle, Washington 98195, USA*

[2] *Department of Physics, Seattle University, Seattle, Washington 98122, USA*

(Dated: February 3, 2017)

Abstract

Background: Knowledge of nucleon structure is today ever more of a precision science, with heightened theoretical and experimental activity expected in coming years. At the same time, a persistent gap lingers between theoretical approaches grounded in Euclidean methods (*e.g.,* lattice QCD, Dyson-Schwinger Equations [DSEs]) as opposed to traditional Minkowski field theories (such as light-front constituent quark models).

Purpose: Seeking to bridge these complementary worldviews, we explore the potential of a *Euclidean constituent quark model* (ECQM). This formalism enables us to study the gluonic dressing of the quark-level axial-vector vertex, which we undertake as a test of the framework.

Method: To access its indispensable elements with a minimum of inessential detail, we develop our ECQM using the simplified quark+scalar diquark picture of the nucleon. We construct a hyperspherical formalism involving polynomial expansions of diquark propagators to marry our ECQM with the results of Bethe-Salpeter Equation (BSE) analyses, and constrain model parameters by fitting electromagnetic form factor data.

Results: From this formalism, we define and compute a new quantity — the *Euclidean density function* (EDF) — an object that characterizes the nucleon's various charge distributions as functions of the quark's Euclidean momentum. Applying this technology and incorporating information from BSE analyses, we find the quenched dressing effect on the proton's axial-singlet charge to be small in magnitude and consistent with zero, while use of recent determinations of unquenched BSEs results in a large suppression.

Conclusions: The scalar quark + diquark ECQM is a step toward a realistic quark model in Euclidean space, and urges additional refinements. The substantial effect we obtain for the impact on the axial-singlet charge of the unquenched dressed vertex compared to the quenched demands further investigation.

* tjhobbs@uw.edu

I. INTRODUCTION

Hadronic physics is presently at an important crossroads. On the one hand, with its advantageous representation of Minkowski field theory, light-front formalism [1–6] has made impressive gains in understanding the proton's flavor and spin structure [7–10]. At much the same time, techniques grounded in Euclidean field theory, such as Lattice QCD [11, 12] and the methodology of Bethe-Salpeter Equations (BSEs) [13–20], continue to unfold an ever more refined picture of the hadronic spectrum, as well as its various excitations and transitions. An effort to reconcile these two families of approaches is therefore more of a crying necessity than ever before. The present analysis represents an initial step to **bridge** this enduring gap by formulating a *Euclidean constituent quark model* (ECQM).

To this end, we craft a simple model in Euclidean space which binds the constituent quark into the nucleon through the exchange of a scalar spectator diquark. While the quark-diquark approach itself is hardly new (such models have an established history in the analyses of both the DIS sector [21–24] and elastic scattering [10]), our specific formulation of a Euclidean constituent quark model has not to our knowledge been previously attempted.

Standard light-front theory [25, 26] extracts bound state properties (*e.g.,* elastic form factors, inelastic structure functions) from overlaps of 3-dimensional light-front wave functions (LFWFs), which are themselves obtained by integrating a 4-dimensional Bethe-Salpeter amplitude over the "minus" components of the internal momenta $k^- \equiv k^0 - k^3$; these in turn provide a means of obtaining form factors and GPDs from constituent quark models [27–30].

Despite the success of methods rooted in constituent quark models, an uncircuitous means of relating them to Euclidean approaches remains lacking. That is, although techniques have been pioneered recently, *e.g.,* involving Euclidean time projections [31] as well as for projecting the pion's Bethe-Salpeter amplitude onto the LF [32], a direct formulation of the quark model in Euclidean space of the type we describe here has not yet been put forth. Such an approach would bridge the complementary worlds of light-front modeling and Euclidean space methods in that it brings the methods of Euclidean field theory to a description of the nucleon in terms of constituent degrees of freedom. The latter is typically developed using Fock space expansions of the nucleon's wave function on the light-front, but through general covariance we can construct a model in Euclidean space with the same ultimate ingredients; in the end, this will permit us to incorporate into the quark-diquark framework the products

of Euclidean DSE analyses such as the vertex dressing function considered in Sect. IV.

The aim of the present article is to do precisely this, producing the aforementioned ECQM. However, the implementation in Euclidean space requires techniques inspired by hyperspherical QED calculations [33–36], which we trace in detail in Sec. III below. Following angular integration of the resulting 4-dimensional amplitudes in Euclidean hyperspherical space, the formalism we develop outputs distributions for the quark-level densities of the proton as functions of the intermediate quark's Euclidean momentum. These latter quantities we designate *Euclidean density functions* (EDFs), and we carry out their evaluation in the sections below.

In the present paper, we test our formalism by performing an analysis of the quark helicity share of the proton's spin by evaluating the flavor-singlet axial charge as spelled out in later sections. The origin of the proton's spin in the angular momentum of its QCD constituents is a problem that has bedeviled hadronic physics ever since the advent of the "spin crisis" in the late 1980s following the revelation [37, 38] of the European Muon Collaboration (EMC) concerning the small size of the proton's integrated spin-dependent structure function, $\int_0^1 g_1^p(x)\,dx = 0.114 \pm 0.012 \pm 0.026$. During the intervening decades, sufficient progress has been made to reduce the crisis to a mere "spin problem" as it is now more commonly known. Even so, the exact interplay of the various relevant dynamics [39–41] remains sufficiently subtle as to prevent an unambiguous reckoning of the multiple effects giving rise to the proton's spin.

Canonically, the spin of the proton is decomposed among contributions from quark and gluon helicity and orbital angular momentum as [42–44]

$$\frac{1}{2} \;=\; \frac{1}{2}\sum_q \Delta q \;+\; L_q \;+\; J_g \;, \tag{1}$$

and the contribution from the total quark helicity $\sum_q \Delta q$ is now understood to represent approximately one third of the total nucleon spin, and has been the focus of intense experimental and theoretical effort [45–49]. Despite recent progress [10], obtaining this result in the context of constituent quark models, including those formulated on the light-front, remains an elusive goal.

For this reason, an assessment of the rôle played by the exchange of nonperturbative gluons in the setting of a constituent quark model could help weigh whether this effect substantially alters the spin decomposition of Eq. (1). To accomplish this, we use the

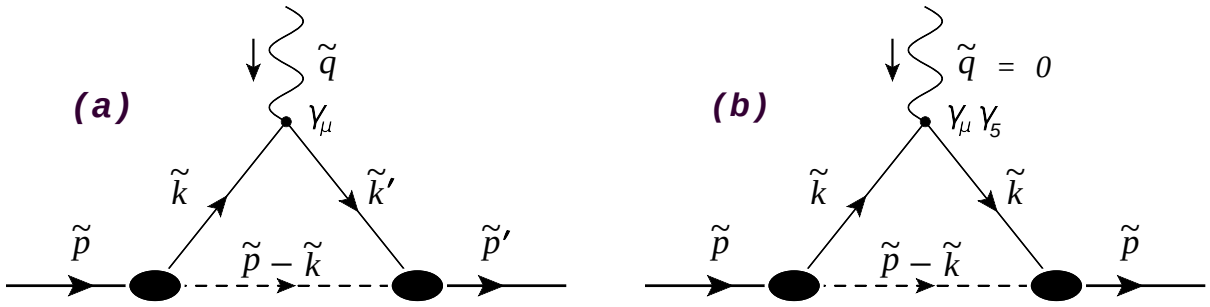

FIG. 1. (Color online) (**a**) The triangle diagram responsible for the nucleon's electromagnetic current J_μ and first nontrivial contribution to $F_{1,2}(\widetilde{q}^2)$. (**b**) The main graph for the quark contributions to the nucleon's axial-singlet charge, a_0. In both cases, solid internal lines represent the propagation of the interacting quark, while the dashed lines are for the scalar spectator diquark. The ovate blobs symbolize our prescription for the momentum dependence of the nucleon-quark-diquark interaction as given by $\varphi(\widetilde{k}^2)$ in Eq. (3).

aforementioned hyperspherical ECQM to incorporate information from BSE analyses on the quark's dressed axial-vector vertex [15, 50–55], ultimately finding a minimal effect with the "quenched" Bethe-Salpeter calculation appropriate for the isovector vertex, but a potentially large suppression once "unquenching" quark loop effects are included.

The remainder of the paper is organized as follows: Sec. II treats the standard covariant approach, with a description of the formalism needed to fit current data in the elastic electromagnetic sector with the bare ECQM in Sec. II A, and a prediction of the proton's axial-singlet charge in Sec. II B; Sec. III describes the hyperspherical formalism. Herein, the basic properties of EDFs are introduced in Sec. III A, and the simplest nontrivial calculation — the EDF for the proton's charge distribution — is given in Sec. III B. Having thus completely determined the details of the bare hyperspherical ECQM, we use it to predict the axial-singlet charge of the proton in Sec. III C, as well as the distribution of this axial charge as a function of the struck quark Euclidean momentum $\widetilde{k}$. In Sec. IV we fold the latest numerical estimates for the soft gluon dressing effect on the axial charge of an individual quark into our formalism, and draw our final conclusions in Sec. V. Lastly, select formulae are postponed to Appendices A and B.

II. THE BARE MODEL: ELECTROMAGNETIC STRUCTURE AND SPIN

A. Electromagnetic form factors

In the quark+scalar diquark picture, computing the Pauli and Dirac form factors $F_1(\widetilde{q}^2)$ and $F_2(\widetilde{q}^2)$ as functions of the spacelike photon virtuality squared $\widetilde{q}^2$ amounts to evaluating the leading triangle diagram in Fig. 1(**a**), which here represents an amplitude formulated in Euclidean space. For this purpose, we take the propagators of the scalar diquark (of mass m_D) and quark (of mass m) to be, respectively,

$$\begin{aligned} D\big([\widetilde{p}-\widetilde{k}]^2\big) &= \frac{1}{[\widetilde{p}-\widetilde{k}]^2+m_D^2}\ , \\ S\big(\widetilde{k}\big) &= \frac{1}{i\widetilde{\not{k}}+m}\ , \end{aligned} \tag{2}$$

where we in general denote Euclidean 4-vectors as $\widetilde{v}_\mu$, and the main prescription-dependent ingredient of the ECQM involves making a formal choice to characterize the binding of the struck constituent quark into the nucleon. To accomplish this, it is necessary to stipulate a relativistic vertex factor for the momentum dependence of the nucleon-quark-diquark interaction, represented by the "blobs" appearing in both panels of Fig. 1. The systematics involved in the implementation of such phenomenological vertex factors have been explored in diverse contexts, including in models of nucleon structure [56–58] and nuclear scattering [59]; in the end, however, we select for simplicity a minimal choice consistent with Lorentz covariance: a scalar function of the quark's Euclidean 4-momentum $\widetilde{k}$ with the general form

$$\varphi(\widetilde{k}^2) \ \equiv \ g\ \left(\frac{\Lambda^2}{\widetilde{k}^2+\Lambda^2}\right)\ . \tag{3}$$

Of course other analytic forms for the vertex function may also be used (*e.g.,* multipoles involving higher powers, or functions of the spectator diquark 4-momentum), but these ultimately lead to qualitatively similar results, and in practice we find use of Eq. (3) simplifies calculations dramatically. For this reason, the remainder of the present analysis is carried out using Eq. (3).

Structurally, the propagators of Eq. (2) are familiar from the Euclidean formalism of Dyson-Schwinger theory [20], which determines the Green's function of a *dressed* quark from its Dyson-Schwinger Equation (DSE), leading to

$$\mathcal{S}\big(\widetilde{k}\big) \ = \ \frac{1}{i\widetilde{\not{k}}\,A\big(\widetilde{k}^2\big)\ +\ B\big(\widetilde{k}^2\big)} \ = \ \frac{\mathcal{Z}\big(\widetilde{k}^2\big)}{i\widetilde{\not{k}}\ +\ \mathcal{M}\big(\widetilde{k}^2\big)}\ , \tag{4}$$

where the nonperturbative dressing functions $A\big(\widetilde{k}^2\big)$ and $B\big(\widetilde{k}^2\big)$ are related to the quark's dynamical mass and wave function renormalization constant via $\mathcal{Z}\big(\widetilde{k}^2\big) = 1/A\big(\widetilde{k}^2\big)$ and $\mathcal{M}\big(\widetilde{k}^2\big) = B\big(\widetilde{k}^2\big)/A\big(\widetilde{k}^2\big)$. In traditional constituent quark models, dynamical chiral symmetry breaking (DCSB) is realized through the large constituent masses of the quark and diquark which emerge effectively after integrating out gluonic degrees of freedom. As a first approximation, we build on this paradigm by ignoring the momentum dependence of the dressed quark's dynamical mass and make the replacement $\mathcal{M}\big(\widetilde{k}^2\big) \to m$ on the grounds that our model is dominated by its behavior in the infrared $\widetilde{k}^2 \approx 0$, as will be apparent in Sect. III. If we similarly ignore the momentum dependence of the renormalization constant $\mathcal{Z}\big(\widetilde{k}^2\big)$ and absorb this quantity into the overall normalization g, we may take the quark propagator to be $\mathcal{S}\big(\widetilde{k}\big) \to S\big(\widetilde{k}\big)$; a similar logic carries through to the diquark, and we therefore proceed with the forms of the propagators given in Eq. (2).

In light of our choice for the nucleon-quark-diquark vertex function, the model parameters in our framework are thus the strength of the nucleon's couplings to its internal quark/diquark degrees of freedom g (which acts as an overall normalization), the constituent masses of the quark and scalar diquark m and m_D, respectively, and the ultraviolet cutoff parameter Λ, all of which we take from fits in the electromagnetic sector. Namely, the form factors $F_{1,2}(\widetilde{q}^2)$ are extracted from the triangle diagram shown in Fig. 1, which gives the extended electromagnetic vertex $\Gamma_\mu\big(\widetilde{p}\,',\widetilde{p}\big)$ of the nucleon as

$$\begin{aligned}\overline{u}(\widetilde{p}\,')\,\gamma_\mu\,u(\widetilde{p}) \;&\longrightarrow\; \overline{u}(\widetilde{p}\,')\,\Gamma_\mu\big(\widetilde{p}\,',\widetilde{p}\big)\,u(\widetilde{p}) \;=\; J_\mu \\ &= \frac{1}{(2\pi)^4}\int d^4\widetilde{k}\;\overline{u}(\widetilde{p}\,')\left(\frac{1}{i\widetilde{\not{k}}\,'+m}\right)\gamma_\mu\left(\frac{1}{i\widetilde{\not{k}}+m}\right)u(\widetilde{p})\left(\frac{\varphi(\widetilde{k}\,'^2)\,\varphi(\widetilde{k}^2)}{[\widetilde{p}-\widetilde{k}]^2+m_D^2}\right)\,,\end{aligned} \tag{5}$$

where $\widetilde{p}$ $\big(\widetilde{p}\,'\big)$ is the intial (final) proton 4-momentum, $\widetilde{k}\,' = \widetilde{k}+\widetilde{q}$, and $\widetilde{p}\,' = \widetilde{p}+\widetilde{q}$. Using the general form of the photon-proton vertex given by Eq. (A10) in App. A, we compute this latter amplitude using standard techniques [60, 61] involving Feynman parameters and momentum shifts to obtain

$$\begin{aligned}F_1(\widetilde{q}^2) \;&=\; \left(\frac{g\Lambda^2}{4\pi}\right)^2\int_0^1 dx\int_0^{1-x}dy\int_0^{1-x-y}dz\int_0^{1-x-y-z}dw \\ &\qquad\times\left(\left[\frac{1}{\Delta^2}\right]^2+2N_1(\widetilde{q}^2)\,\left[\frac{1}{\Delta^2}\right]^3\right)\,,\end{aligned} \tag{6}$$

$$F_2(\widetilde{q}^2) \;=\; 2\left(\frac{g\Lambda^2}{4\pi}\right)^2\int_0^1 dx\int_0^{1-x}dy\int_0^{1-x-y}dz\int_0^{1-x-y-z}dw\;N_2(z)\,\left[\frac{1}{\Delta^2}\right]^3\,, \tag{7}$$

in which

$$N_1(\widetilde{q}^2) \;=\; \big(m+zM\big)^2 - (x+w)\,\big(1-x-z-w\big)\,\widetilde{q}^2\;, \tag{8}$$

$$N_2(z) \;=\; 2M\,(1-z)\,\big(m+zM\big)\;, \tag{9}$$

$$\begin{aligned}\Delta^2 \;=\; & (x+w)\,\big(1-x-z-w\big)\,\widetilde{q}^2 + (x+y)\,m^2 + z m_D^2 \\ & - z\,(1-z) M^2 + (1-x-y-z)\,\Lambda^2\;. \end{aligned} \tag{10}$$

Above, M is the mass of the on-shell nucleon, and we have made use of the Euclidean Gordon Identity given by Eq. (A9) to decompose the amplitude of Eq. (5) into separate Pauli and Dirac components *à la* Eq. (A10).

With these explicit expressions for F_1 and F_2, it is simple to construct the familiar Sach's parametrization of the nucleon's electromagnetic form factors:

$$\begin{aligned} G_E(\widetilde{q}^2) \;&\equiv\; F_1(\widetilde{q}^2) \;-\; \frac{\widetilde{q}^2}{4M^2}\,F_2(\widetilde{q}^2)\;, \\ G_M(\widetilde{q}^2) \;&\equiv\; F_1(\widetilde{q}^2) \;+\; F_2(\widetilde{q}^2)\;, \end{aligned} \tag{11}$$

and we may determine the model parameters by fitting these expressions to experimental data on the proton. For this purpose, we treat the phenomenological parametrization of Kelly [62] as a proxy for the world's experimental data and global fits thereof [63, 64], rather than preferencing individual sets; we may then minimize the numerical badness-of-fit measure

$$\chi^2 \;\equiv\; \frac{1}{2n_p}\,\sum_{i=1}^{n_p}\left(\frac{G_E(\widetilde{q}_i^2) - G_E^{phen.}(\widetilde{q}_i^2)}{G_E^{phen.}(\widetilde{q}_i^2)}\right)^2 \;+\; \left(\frac{G_M(\widetilde{q}_i^2) - G_M^{phen.}(\widetilde{q}_i^2)}{G_M^{phen.}(\widetilde{q}_i^2)}\right)^2\;. \tag{12}$$

This analysis is intended as a demonstration of the basic foundations of a ECQM, and hence we restrict our attention to the proton. Evaluating the Ward Identity based upon the triangle diagram of Fig. 1(**a**) gives $\widetilde{q}\cdot J = 0$, thus proving gauge invariance and guaranteeing the conservation of charge within the quark-diquark picture. In the model under consideration, wherein a quark interacts with an external electromagnetic current while the scalar diquark is a recoiling spectator, the struck quark carries the full charge of the proton, and the formulation as presented here is sufficient. On the other hand, to describe experimental information on the neutron and proton simultaneously, a more elaborate spin-flavor wave function is necessary, as well as additional axial-vector modes for the spectator diquark as studied on the light-front in Ref. [10], for instance. We regard such embellishments as beyond the scope of this article, and delay them for future analysis.

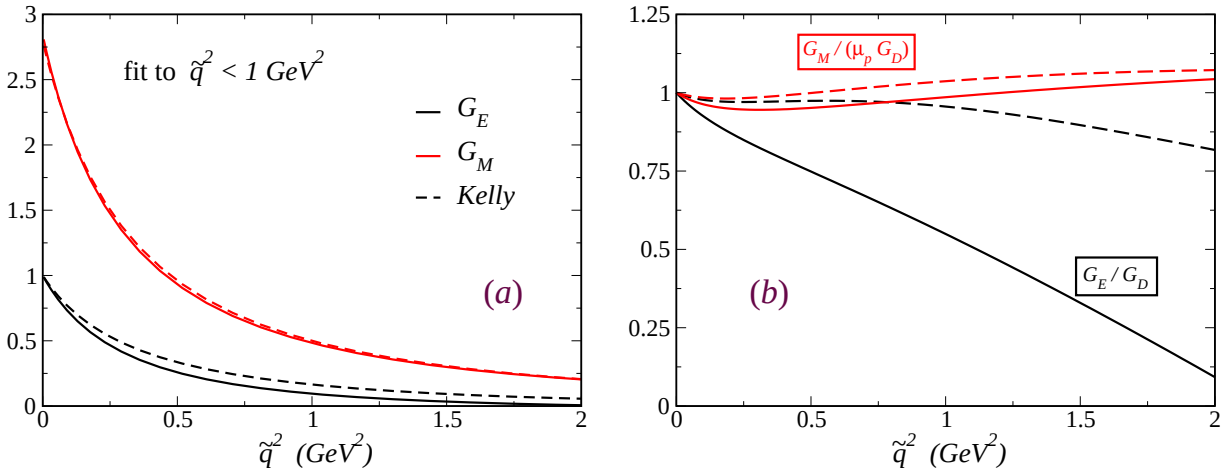

FIG. 2. (Color online) (**a**) A plot of the fitted electromagnetic form factors $G_{E,M}(\widetilde{q}^2)$, where we constrain fits with the phenomenological parametrization of Kelly [62] for $\widetilde{q} \leq 1$ GeV. Here, solid lines give the result of our fitted model for the parameters listed in Table I, while the dashed lines are the phenomenological fits of Ref. [62], with G_E given in black and G_M in red in both cases. (**b**) A similar comparison, but in this case for the form factor ratios with respect to the well-known dipole parametrization [62] $G_D(\widetilde{q}^2) \equiv (1 + \widetilde{q}^2/\Lambda_D^2)^{-2}$, where $\Lambda_D^2 = 0.71$ GeV^2.

We note that to ensure the numerical validity of the hyperspherical Euclidean space formalism given later in Sec. III, we in practice find it necessary to constrain the value of the diquark mass to be no less than that of the proton, $m_D \geq M$, while the other parameters are allowed to float freely over a broad range. This condition is a generic artifact of hyperspherical techniques as applied to massive theories [35], and for QED can be circumvented with an appropriate deformation of the integration contour in the complex $\widetilde{k}^2$ plane. For the amplitudes under consideration here, however, such an approach meets further complications due to the presence of quark denominators $\sim(\widetilde{k}^2 + m^2)^{-2}$, which can produce singularities in the timelike region $\widetilde{k}^2 < 0$ into which the contour over $\widetilde{k}^2$ is deformed; we therefore opt for the simpler $m_D \geq M$ condition in this initial study. We note of course that this procedure confers the added benefit of simulating the effects of a confining potential in the sense that the nucleon is thereby prohibited from decaying into its constituents ($m + m_D \geq M$, for any choice of m).

Also, for the sake of describing the nucleon axial-singlet charge (which is defined at $\widetilde{q}^2 = 0$) we concentrate our fits at low photon virtualities, and hence only constrain them

χ^2	m	m_D	Λ	g	μ_p (μ_N)	a_0	$M^1_{\overline{f}_1}$	$M^1_{\overline{a}_0}$
0.00297	0.637	0.947	0.228	79.104	2.843	0.784	0.1985	0.08125

TABLE I. The collection of parameters that follow from constraining our model to the proton electromagnetic form factors G_E and G_M at low $\widetilde{q} \leq 1$ GeV as given by [62]. The parameters given in the first enclosed box are fitted directly, while those in the open box at the far right are predicted by the fitted model. Note that the interaction strength g and bare axial-singlet charge a_0 determined in Sec. II are dimensionless, while the final two columns give the first moments of the electric and axial-singlet quark charge EDFs $M^1_{\overline{f}_1}$ and $M^1_{\overline{a}_0}$ in GeV^2; units elsewhere are in GeV unless otherwise noted.

with experimental information for $\widetilde{q} \leq 1$ GeV. Doing so, we find that fitting our scalar diquark model to the Kelly prediction for G_E and G_M at 5 uniformly-chosen points in the domain $0 \leq \widetilde{q} \leq 1$ GeV [*i.e.,* $n_p = 5$ in Eq. (12) above] results in the description plotted in Fig. 2, which corresponds to a χ^2 per datum of 0.003 for the specific parameter values given in Table I. The numerical values of the fitting parameters imply a mass for the diquark comparable to that of the nucleon (consistent with Faddeev Equation studies, *e.g.,* Ref. [65]), and a rather large constituent quark mass $m \sim 600$ MeV.

In particular, the two panels of Fig 2 compare this fitted model to the parametrization of Ref. [62] for the proton, both at the level of the separate form factors G_E and G_M themselves (**a**), as well as for the instructive ratios (**b**) with respect to the one-parameter dipole approximation [62] $G_D(\widetilde{q}^{\,2}) \equiv (1 + \widetilde{q}^{\,2}/\Lambda_D^2)^{-2}$, with $\Lambda_D^2 = 0.71$ GeV^2 — the latter serving to draw attention to subtleties in the form factors' behavior at larger $\widetilde{q}^{\,2}$. In both panels also, solid curves represent the output of our fitted model, while dashed lines are the prediction of Ref. [62].

For the region of interest ($\widetilde{q}^2 \gtrsim 0$), fitted results agree especially well with G_M, matching its qualitative dependence on $\widetilde{q}^2$ quite closely; for G_E, however, the agreement is somewhat weaker, as especially highlighted by the relatively steep downturn of the solid-black curve of Fig. 2(**b**). At the same time, we adjudicate the better-than $\sim 10\%$ agreement at lowest $\widetilde{q}^{\,2} \lesssim 0.2$ GeV^2 for G_E and percent-level agreement for G_M to be fully adequate for our demonstration of the hyperspherical formalism here, which we pursue in the following

sections only for quantities defined in the real limit, $\widetilde{q}^{\,2}=0$, including the axial charge a_0.

B. Axial-singlet charge

The total quark helicity contribution to the nucleon spin in Eq. (1) may be identified with the matrix element for the axial-singlet charge of the proton [66], $a_0=\sum_q \Delta q$, which we write explicitly as

$$2M\widetilde{S}_\mu\, a_0 \;\equiv\; \langle \widetilde{p},s|\;\overline{q}\,\gamma_\mu\gamma_5\,q\;|\widetilde{p},s\rangle\;, \qquad \widetilde{S}_\mu \;\equiv\; \frac{1}{2M}\,\overline{u}(\widetilde{p})\,\gamma_\mu\gamma_5\,u(\widetilde{p})\;, \tag{13}$$

in which $\widetilde{S}_\mu$ represents the nucleon's Euclidean spin 4-vector, which obeys $\widetilde{S}\cdot\widetilde{p}=0$ and $\widetilde{S}^2=-1$. For the non-pointlike proton basis states consistent with the bare quark+diquark picture, the matrix element of Eq. (13) can be realized diagrammatically in a triangle graph akin to that which produced Eqs. (6) and (7) for the proton's electromagnetic substructure — albeit with the appropriate $\sim\gamma_\mu\gamma_5$ operator entering at the axial current-quark vertex. This is shown explicitly in Fig. 1(**b**), wherein $\widetilde{p}\,'=\widetilde{p}$, as is relevant for the axial-singlet charge defined at $\widetilde{q}=0$. Using our established Euclidean conventions, this then gives the amplitude

$$2M\widetilde{S}_\mu\, a_0 \;=\; \frac{1}{(2\pi)^4}\int d^4\widetilde{k}\;\overline{u}(\widetilde{p})\left(\frac{1}{i\widetilde{\not{k}}+m}\right)\;\gamma_\mu\gamma_5\;\left(\frac{1}{i\widetilde{\not{k}}+m}\right)u(\widetilde{p})\left(\frac{|\varphi(\widetilde{k}^2)|^2}{[\widetilde{p}-\widetilde{k}]^2+m_D^2}\right)\;. \tag{14}$$

Thus we can follow a procedure similar to that used in the electromagnetic sector to compute the bare (*i.e., undressed*) quark + scalar diquark model prediction for the proton's axial-singlet charge, keeping in mind that we will ultimately match our ECQM formalism to the standard calculation in Sec. III C, constituting a vital test. We find

$$\begin{aligned} 2M\widetilde{S}_\mu a_0 \;=\; & \Gamma(5)\,\frac{g^2\Lambda^4}{(2\pi)^4}\int\frac{d^4\widetilde{l}}{(\widetilde{l}^2+\Delta^2)^5}\int dx\,dy\,dz\;\; xy\;\delta\big(1-[x+y+z]\big) \\ & \times\;\overline{u}(\widetilde{p})\left(-i(\widetilde{\not{l}}+z\widetilde{\not{p}})+m\right)\gamma_\mu\gamma_5\left(-i(\widetilde{\not{l}}+z\widetilde{\not{p}})+m\right)u(\widetilde{p})\;; \end{aligned} \tag{15}$$

again using textbook [60] covariant methods, this can be manipulated to yield

$$a_0 \;=\; -\left(\frac{g\Lambda^2}{4\pi}\right)^2\int_0^1 dy\int_0^{1-y}dz\;y(1-y-z)\left(\left[\frac{1}{\Delta^2}\right]^2-2(m+zM)^2\left[\frac{1}{\Delta^2}\right]^3\right)\;, \tag{16}$$

where here the explicit expression for the denominator in terms of masses and Feynman parameters is

$$\Delta^2 \;=\; (1-y-z)m^2+y\Lambda^2+zm_D^2-z(1-z)M^2\;, \tag{17}$$

and we have implemented the shift $\widetilde{k}_\mu \to \widetilde{l}_\mu = \widetilde{k}_\mu - z\,\widetilde{p}_\mu$, and made use of Eq. (A8). Thus, Eq. (16) is fully defined, and may be computed with the model parameters determined in the electromagnetic sector — *i.e.,* the values contained within the inner box of Table I. Inserting these, we get $a_0 = 0.784$, which we also report in the rightmost partition of Table I. We reproduce this value via hyperspherical techniques in Sec. III C.

III. HYPERSPHERICAL FORMALISM

A. Euclidean density function

Here we introduce the framework necessary to obtain 4-dimensional Euclidean quark-level densities — for the proton's electromagnetic charge in Sec. III B, and its axial-singlet charge in Sec. III C.

Formally, we seek 4-dimensional densities dependent on the interacting quark's Euclidean momentum $\widetilde{k}$. Such quantities would be analogous to the squares of Bethe-Salpeter wave functions $\Psi(k;p)$ from which LFWFs can be derived via the appropriate integral over $\int dk^-$ at fixed LF time [25, 26] as described in Sec. I. Properly formulated, in our case these density functions will allow the recovery of bulk properties of the nucleon from radial integrals in Euclidean space governed by the parameters of a constituent quark model. That is, the total nucleon charge and axial-singlet charge follow from the zeroth moment of the *Euclidean density functions* (EDFs) $\overline{f}_1(\widetilde{k}^2)$ and $\overline{a}_0(\widetilde{k}^2)$, respectively:

$$F_1(\widetilde{q}^2{=}0) \;=\; \int d\widetilde{k}^2\; \overline{f}_1(\widetilde{k}^2)\;, \tag{18}$$

$$a_0 \;=\; \int d\widetilde{k}^2\; \overline{a}_0(\widetilde{k}^2)\;, \tag{19}$$

where the integrations over $\int d\widetilde{k}^2$ remain after summing over angles, and EDFs for other charges may also be constructed. In fact, inasmuch as EDFs enjoy the proper support (in this case, vanishing in the limit $\widetilde{k}^2 \to \infty$), their lowest moments in $\widetilde{k}^2$ may also be computed:

$$M^n_{\overline{f}_1} \;\equiv\; \int d\widetilde{k}^2\; \left(\widetilde{k}^2\right)^n\; \overline{f}_1(\widetilde{k}^2)\;, \tag{20}$$

$$M^n_{\overline{a}_0} \;\equiv\; \int d\widetilde{k}^2\; \left(\widetilde{k}^2\right)^n\; \overline{a}_0(\widetilde{k}^2)\;, \tag{21}$$

for which the choice $(n = 0)$ corresponds to the expressions in Eqs. (18) and (19), while the nontrivial first moments $(n = 1)$, corresponding to $M^1 \sim \langle\widetilde{k}^2\rangle$, provide information on the

mean $\widetilde{k}^2$ of the electromagnetic and axial-charge densities. We determine these explicitly in Secs. III B and III C below, and ultimately plot their associated integrands in Fig. 3.

Pending this more detailed calculation, the proton's charge EDF $\overline{f}_1(\widetilde{k}^2)$ may be described to first approximation in the spirit of Feynman *et al.* [67], using a Euclideanized Gaussian wave function $\psi(\widetilde{k}^2) \sim \exp(-R^2\widetilde{k}^2/2)$:

$$\begin{aligned} F_1(\widetilde{q}^2=0) \;&=\; \frac{1}{(2\pi)^4}\int d^4\widetilde{k}\;\left|\psi(\widetilde{k}^2)\right|^2 \;=\; 1 \\ \rightarrow\;\; \psi(\widetilde{k}^2) \;&=\; \left(4\pi R^2\right)\,\exp\left\{-\frac{1}{2}\,R^2\,\widetilde{k}^2\right\}\;, \end{aligned} \tag{22}$$

for which the dependence of the wave function on the quark momentum $\widetilde{k}$ is governed purely by the proton RMS radius, $R \equiv \langle r_p^2\rangle^{1/2} \approx 0.88\,\text{fm} = 1/(0.227\,\text{GeV})$ [68]. Noting Eq. (B2), we conclude

$$\overline{f}_1^{\,\text{WF}}(\widetilde{k}^2) \;=\; R^4\,\widetilde{k}^2\;\exp\left\{-R^2\,\widetilde{k}^2\right\}\;, \tag{23}$$

a simple result to which we compare the model results of Secs. III B and III C below as an instructive benchmark. Plotting the integrand $2\widetilde{k}\,\overline{f}_1^{\,\text{WF}}(\widetilde{k}^2)$ of $F_1(0)$ against $\widetilde{k}$ in Fig. 3, the resulting distribution peaks predictably near $\widetilde{k} \gtrsim 0.2$ GeV due to our numerical choice of R, but then has a sharper momentum dependence at higher $\widetilde{k}$ not found for the more realistic model calculations presented below; this fact alone highlights the necessity for the more detailed hyperspherical treatment of nucleon spin structure outlined in Secs. III B–III C.

Ultimately, in a utilitarian sense the EDFs of Eqs. (18) and (19) also permit an interface with the output of traditional Euclidean field-theoretic approaches, as emphasized in Sec. I. Whereas the formalism of Sec. II is adequate for the determination of the total proton charge and helicity in the bare quark model, we ultimately wish to absorb the results of BSE analyses into our ECQM to assess the gluon dressing effect. For this purpose, however, BSEs describe the impact of soft gluon exchange in the form of vertex functions of the quark's Euclidean momentum, and there is no straightforward way to incorporate such quantities into the bare calculation of Sec. II B, especially given the reliance of the latter upon shifting loop momenta away from those given in Fig. 1(**b**).

On the other hand, given their status as vertex functions of the quark momentum, BSE results may be incorporated directly into the integrated EDFs typified by Eq. (19) as quark momentum-dependent smearing functions $f_g(\widetilde{k}^2)$. It is precisely such a scheme that we pursue here for the quark helicity contribution to the nucleon spin, a_0. Thus, with the

EDF $\overline{a}_0(\widetilde{k}^2)$ and the smearing function $f_g(\widetilde{k}^2)$ for the gluon-dressing effect in hand, one may compute the impact of soft gluon exchange upon the total quark helicity contribution to the proton spin, leading to a corrected axial-singlet charge

$$a_0' \;=\; \int d\widetilde{k}^2\; \overline{a}_0(\widetilde{k}^2)\; f_g(\widetilde{k}^2)\;, \tag{24}$$

where in practice we identify the gluonic smearing function with the nonperturbative axial-vector vertex factor of BSE studies, $f_g(\widetilde{k}^2) = F_R(\widetilde{k}^2, 0)$, which we take from Refs. [53, 55] and describe in greater detail in Sec. IV. Moreover, we point out that assuming the perturbative result expected to hold at $\widetilde{k} \gg 0$ for the gluon dressing function, $f_g(\widetilde{k}^2) = 1$, in Eq. (24) simply recovers the bare ECQM calculation given by Eq. (19).

We can in fact achieve the specifics of the general formalism described above, and this amounts to the main result of the present paper. We derive the EDFs of Eqs. (18) and (19) by closely following the analogous calculation for the hadronic vacuum polarization effect in the muon's anomalous magnetic moment [33]; viz., we now evaluate Eq. (5) for $\widetilde{p}\,' = \widetilde{p}$ in Sec. III B and Eq. (14) in Sec. III C using a hyperspherical formalism originally adapted to QED [34–36].

B. Quark charge distribution

The hyperspherical formalism we describe below is of sufficient generality that it may be deployed in the evaluation of various Euclidean momentum distributions. As an initial demonstration, however, we highlight the calculation of the EDF for the proton's electric charge: *i.e.,* the integrand leading to $F_1(\widetilde{q}^{\,2} = 0)$ of Eq. (18). As will be the case for the subsequent determination of $\overline{a}_0(\widetilde{k})$, we start at amplitude-level, in this case with Eq. (5), which at $\widetilde{q}^2 = 0$ yields

$$2i\,\widetilde{p}_\mu\, F_1(0) \;=\; \frac{1}{(2\pi)^4} \int d^4\tilde{k}\; \overline{u}(\widetilde{p}) \left(\frac{1}{i\widetilde{\not{k}} + m}\right) \gamma_\mu \left(\frac{1}{i\widetilde{\not{k}} + m}\right) u(\widetilde{p}) \left(\frac{\left|\varphi(\widetilde{k}^2)\right|^2}{[\widetilde{p} - \widetilde{k}]^2 + m_D^2}\right) \tag{25}$$

$$= \frac{g^2\Lambda^4}{(2\pi)^4} \int d\widetilde{k}^4\; \frac{\overline{u}(\widetilde{p}) \left[-2\widetilde{\not{k}}\widetilde{k}_\mu + \left(\widetilde{k}^2 + m^2\right)\gamma_\mu - im\{\gamma_\mu, \widetilde{\not{k}}\}\right] u(\widetilde{p})}{(\widetilde{k}^2 + m^2)^2\,(\widetilde{k}^2 + \Lambda^2)^2\,\left([\widetilde{p} - \widetilde{k}]^2 + m_D^2\right)}\;, \tag{26}$$

where we have again used Eq. (A10) for the general form of the electromagnetic vertex given in App. A. To apply the hyperspherical formalism, we must express the numerator algebra

leading to $F_1(0)$ in terms of inner products. For this example, we achieve this by contracting both sides of Eq. (26) with $\widetilde{p}_\mu$ and using the identities of App. A, which brings us to the expression

$$F_1(0) \;=\; \frac{g^2\Lambda^4}{(2\pi)^4}\int d\widetilde{k}^4\,\frac{\widetilde{k}^2+m^2-\frac{2}{\widetilde{p}^2}\left(\widetilde{p}\cdot\widetilde{k}\right)^2+\frac{2}{\widetilde{p}^2}mM\left(\widetilde{p}\cdot\widetilde{k}\right)}{(\widetilde{k}^2+m^2)^2\,(\widetilde{k}^2+\Lambda^2)^2\,\Big([\widetilde{p}-\widetilde{k}]^2+m_D^2\Big)}\;. \tag{27}$$

More critically, rather than shifting away the term in the denominator $\sim(\widetilde{p}\cdot\widetilde{k})$ as in the standard covariant calculations involving Feynman parameters [Eqs. (6) – (7) and (16)], we instead make an expansion of the scalar diquark propagator:

$$\frac{1}{[\widetilde{p}-\widetilde{k}]^2+m_D^2} \;=\; \frac{Z_{pk}}{\widetilde{p}\widetilde{k}}\sum_{n=0}^{\infty}\Big(Z_{pk}\Big)^n C_n\big(\hat{p}\cdot\hat{k}\big)\;, \tag{28}$$

where explicitly,

$$Z_{pk} \;\equiv\; \frac{1}{2\widetilde{p}\,\widetilde{k}}\Big(\widetilde{p}^2+\widetilde{k}^2+m_D^2-\sqrt{(\widetilde{p}^2+\widetilde{k}^2+m_D^2)^2-4\widetilde{p}^2\widetilde{k}^2}\Big)\;, \tag{29}$$

and we sometimes find it convenient to work in terms of the dimensionful object $Z\equiv Z_{pk}/\widetilde{p}\widetilde{k}$. In Eq. (28), the C_n are *Gegenbauer polynomials* with the normalization and orthogonality properties described in App. B, and $\hat{p}$ is a unit vector in Euclidean space in the direction of $\widetilde{p}_\mu$. We can exploit these properties in App. B to perform the necessary angular integrations by first rendering the numerator of Eq. (27) in terms of a linear combination of the Gegenbauer polynomials

$$\left(\widetilde{p}\cdot\widetilde{k}\right) \;=\; \frac{\widetilde{p}\,\widetilde{k}}{2}\,C_1(\hat{p}\cdot\hat{k})\;, \tag{30}$$

$$\left(\widetilde{p}\cdot\widetilde{k}\right)^2 \;=\; \frac{1}{4}\,\widetilde{p}^2\,\widetilde{k}^2\,\Big(C_2(\hat{p}\cdot\hat{k})+C_0(\hat{p}\cdot\hat{k})\Big)\;. \tag{31}$$

Inserting everything into Eq. (27) and using Eq. (B2) then results in

$$\begin{aligned}F_1(0) \;=\;& \frac{g^2\Lambda^4}{(2\pi)^4}\int\frac{d\widetilde{k}^2}{2}\,\frac{\widetilde{k}^2 Z}{(\widetilde{k}^2+m^2)^2\,(\widetilde{k}^2+\Lambda^2)^2}\int d\Omega_{\hat{k}}\,\Big(\sum_{n=0}^{\infty}\big(\widetilde{p}\,\widetilde{k}\,Z\big)^n C_n(\hat{p}\cdot\hat{k})\Big)\\ &\times\;\left(-\frac{\widetilde{k}^2}{2}\big(C_2(\hat{p}\cdot\hat{k})+C_0(\hat{p}\cdot\hat{k})\big)+\frac{mM}{\widetilde{p}^2}\widetilde{p}\,\widetilde{k}\,C_1(\hat{p}\cdot\hat{k})+(m^2+\widetilde{k}^2)\,C_0(\hat{p}\cdot\hat{k})\right)\;;\end{aligned} \tag{32}$$

and we may use Eq. (B3) to evaluate the angular integral $\int\Omega_{\hat{k}}$. Before doing so, however, it is imperative to note that Eq. (32) is defined in general for spacelike 4-momenta (including the external nucleon 4-momentum $\widetilde{p}^2\geq 0$). It is therefore necessary to perform an analytic

continuation of the proton momentum into the timelike region where it is explicitly on-shell and thus physical: $\widetilde{p}^2 = -M^2$. By merit of our requirement that $m_D \geq M$, the integration contour $\widetilde{k}^2 \in [0, \infty)$ remains unmenaced by branch points or singularities, and the nucleon momentum may be straightforwardly continued to $\widetilde{p} \to iM$. Doing so after evaluating the angular integrals, we finally obtain

$$F_1(0) \;=\; \left(\frac{g\Lambda^2}{4\pi}\right)^2 \int d\widetilde{k}^2 \, \frac{\widetilde{k}^2 \overline{Z}}{(\widetilde{k}^2 + m^2)^2 \, (\widetilde{k}^2 + \Lambda^2)^2} \left(\frac{\widetilde{k}^2}{2} + \frac{M^2}{2} \big(\widetilde{k}^2 \overline{Z}\big)^2 + mM \widetilde{k}^2 \overline{Z} + m^2 \right) , \tag{33}$$

in which $\overline{Z}$ represents the analytic continuation of the rational function Z of Eq. (29), given explicitly by

$$\overline{Z} \;=\; -\frac{1}{2M^2 \widetilde{k}^2} \left(\widetilde{k}^2 + \delta^2 - \sqrt{(\widetilde{k}^2 + \delta^2)^2 + 4M^2 \widetilde{k}^2} \right) , \tag{34}$$

having defined the shorthand $\delta^2 \equiv m_D^2 - M^2$.

It is notable also that the expression given in Eq. (33) constitutes an important check of the hyperspherical formalism which we use in Sec. III C below for a_0, and one may straightforwardly verify that it yields $F_1(0) = 1$ for the parameters of Table I. From it, we may at last extract the Euclidean density function $\overline{f}_1(\widetilde{k}^2)$ for the proton's quark-level charge through direct matching with Eq. (18),

$$\overline{f}_1(\widetilde{k}^2) \;=\; \left(\frac{g\Lambda^2}{4\pi}\right)^2 \frac{\widetilde{k}^2 \overline{Z}}{(\widetilde{k}^2 + m^2)^2 \, (\widetilde{k}^2 + \Lambda^2)^2} \left(\frac{\widetilde{k}^2}{2} + \frac{M^2}{2} \big(\widetilde{k}^2 \overline{Z}\big)^2 + mM \widetilde{k}^2 \overline{Z} + m^2 \right) ; \tag{35}$$

we plot this EDF in Fig. 3 alongside the analoguous quantity for the axial-singlet charge $\overline{a}_0(\widetilde{k}^2)$ derived in Sec. III C below.

Having determined the quark-level EDF for the proton's electric charge in Eq. (35), we may use this result to evaluate higher moments of the charge distribution given in Eq. (20):

$$M^1_{\bar{f}_1} \;=\; 0.1985 \text{ GeV}^2 \, . \tag{36}$$

In this case, this value corresponds roughly to the center of the peak of the heavy-solid line in Fig. 3; more directly, we also plot the integrand over $\widetilde{k}$ for the moment $M^1_{\bar{f}_1}$ as the thin-solid line, multiplied by a factor of 2 for ease of comparison.

C. Quark helicity

While the formalism in Sec. II B above was sufficient to determine the bare quark helicity contribution to the proton axial-singlet charge a_0, we must ultimately interface our quark-

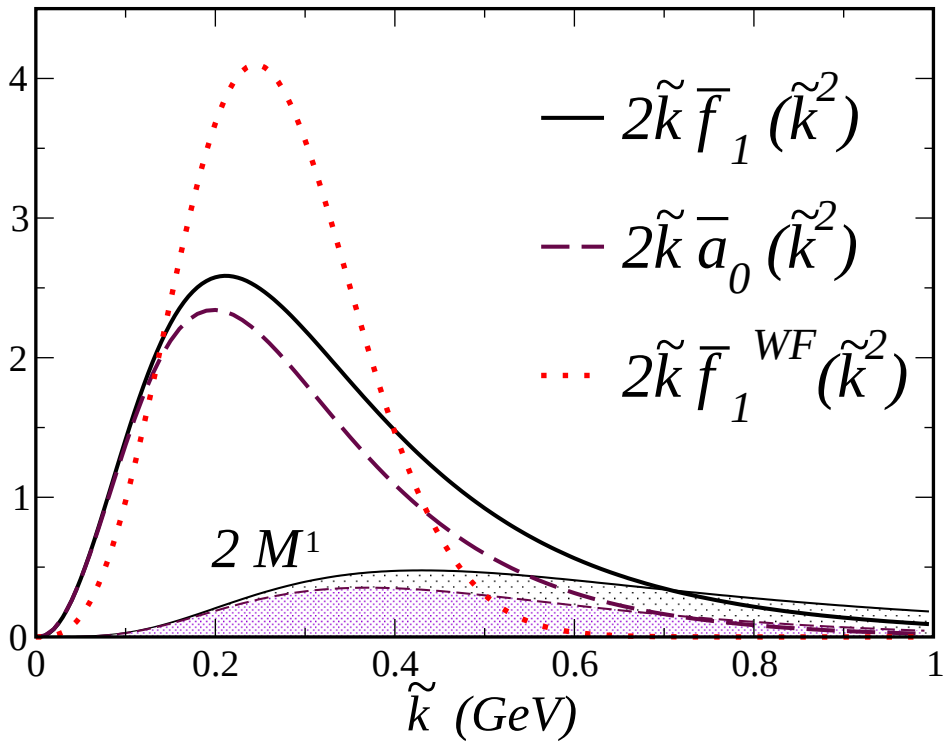

FIG. 3. (Color online) A comparison of EDFs for the proton's charge $2\widetilde{k}\,\overline{f}_1(\widetilde{k}^2)$ [Eq. (35), black-solid] and axial-singlet charge $2\widetilde{k}\,\overline{a}_0(\widetilde{k}^2)$ [Eq. (42), maroon-dashed] carried by the struck quark in the scalar diquark ECQM as functions of its Euclidean momentum $\widetilde{k}$; for illustration, we contrast these with the result of using the Gaussian wave function, $2\widetilde{k}\,\overline{f}_1^{\rm WF}(\widetilde{k}^2)$ from Eq. (23) [red-dotted]. The thin lines and associated shaded regions at bottom correspond to the integrands of these distributions' first moments in $\widetilde{k}^2$, *i.e.*, $M^1 \sim \langle\widetilde{k}^2\rangle$ of Eqs. (20) and (21). Note that these latter moments have been rescaled by a factor of 2 for comparison.

diquark framework with the results of BSE analyses to estimate the gluon dressing effect as mentioned above. In this case, the BSE calculations we aim to incorporate are $\widetilde{k}$-dependent vertex factors as noted in Sec. III A, and thus we require an axial charge momentum distribution along the lines of Eq. (35) to evaluate Eq. (24).

Hence, analogously to the calculation in Sec. III B, we now proceed by contracting both sides of Eq. (14) with the nucleon spin 4-vector $\widetilde{S}_\mu$ to obtain

$$\begin{aligned} 2Ma_0 &= -\frac{g^2\Lambda^4}{(2\pi)^4}\int d^4\widetilde{k}\,\frac{\widetilde{S}_\mu\,\overline{u}(\widetilde{p})\left(-i\widetilde{\not{k}}+m\right)\gamma_\mu\gamma_5\left(-i\widetilde{\not{k}}+m\right)u(\widetilde{p})}{(\widetilde{k}^2+m^2)^2\,(\widetilde{k}^2+\Lambda^2)^2\left([\widetilde{p}-\widetilde{k}]^2+m_D^2\right)} \\ &= -\frac{g^2\Lambda^4}{(2\pi)^4}\int d^4\widetilde{k}\,\frac{2M\left(\,2(\widetilde{S}\cdot\widetilde{k})^2+(m^2-\widetilde{k}^2)\widetilde{S}^2\,\right)\;-\;4m(\widetilde{p}\cdot\widetilde{k})}{(\widetilde{k}^2+m^2)^2\,(\widetilde{k}^2+\Lambda^2)^2\left([\widetilde{p}-\widetilde{k}]^2+m_D^2\right)}\,, \end{aligned} \tag{37}$$

and here we require an additional inner product:

$$(\widetilde{S}\cdot\widetilde{k})^2 \;=\; \frac{1}{4}\,\widetilde{S}^2\widetilde{k}^2\,\Big(C_2(\hat{S}\cdot\hat{k})+C_0(\hat{S}\cdot\hat{k})\Big)\;. \tag{38}$$

Using this and Eq. (30) to re-write the inner products of Eq. (37) above, we incorporate the polynomial expansion for $\big(\,[\widetilde{p}-\widetilde{k}]^2+m_D^2\,\big)^{-1}$; here this leads to

$$\begin{aligned} a_0 \;&=\; \frac{g^2\Lambda^4}{(2\pi)^4}\int\frac{d\widetilde{k}^2}{2}\,\frac{\widetilde{k}^2 Z}{(\widetilde{k}^2+m^2)^2\,(\widetilde{k}^2+\Lambda^2)^2}\int d\Omega_{\hat{k}}\,\Big(\sum_{n=0}^{\infty}\big(\widetilde{p}\,\widetilde{k}\,Z\big)^n C_n(\hat{p}\cdot\hat{k})\Big) \qquad (39)\\ &\quad\times\;\Big(\frac{\widetilde{k}^2}{2}\big(C_2(\hat{S}\cdot\hat{k})+C_0(\hat{S}\cdot\hat{k})\big)-\frac{m}{M}\,\widetilde{p}\,\widetilde{k}\,C_1(\hat{p}\cdot\hat{k})+(m^2-\widetilde{k}^2)\,C_0(\hat{S}\cdot\hat{k})\Big)\\ &=\;\Big(\frac{g\Lambda^2}{4\pi}\Big)^2\int d\widetilde{k}^2\,\frac{\widetilde{k}^2 Z}{(\widetilde{k}^2+m^2)^2\,(\widetilde{k}^2+\Lambda^2)^2}\\ &\quad\times\;\Big(\frac{\widetilde{k}^2}{2}\big(\widetilde{p}\,\widetilde{k}\,Z\big)^2\frac{C_2(\hat{S}\cdot\hat{p})}{3}-\frac{m}{M}\,\widetilde{p}\,\widetilde{k}\,\big(\widetilde{p}\,\widetilde{k}\,Z\big)\frac{C_1(\hat{p}\cdot\hat{p})}{2}+(m^2-\frac{\widetilde{k}^2}{2})\,C_0(\hat{S}\cdot\hat{p})\Big)\;. \qquad (40)\end{aligned}$$

As before, we analytically extend $\widetilde{p}$ into the timelike region where it is on-shell, leading to

$$a_0 \;=\; \Big(\frac{g\Lambda^2}{4\pi}\Big)^2\int d\widetilde{k}^2\,\frac{\widetilde{k}^2\overline{Z}}{(\widetilde{k}^2+m^2)^2\,(\widetilde{k}^2+\Lambda^2)^2}\,\left(-\frac{\widetilde{k}^2}{2}+\frac{M^2}{6}\big(\widetilde{k}^2\overline{Z}\big)^2+mM\widetilde{k}^2\overline{Z}+m^2\right)\;, \tag{41}$$

and $\overline{Z}$ is again given by the expression in Eq. (34). Lastly, we deduce the EDF appearing in Eq. (19) [and Eq. (24)] from Eq. (41) by simple matching, as had been done for $\bar{f}_1(\widetilde{k}^2)$:

$$\overline{a}_0(\widetilde{k}^2) \;=\; \Big(\frac{g\Lambda^2}{4\pi}\Big)^2\,\frac{\widetilde{k}^2\overline{Z}}{(\widetilde{k}^2+m^2)^2\,(\widetilde{k}^2+\Lambda^2)^2}\,\left(-\frac{\widetilde{k}^2}{2}+\frac{M^2}{6}\big(\widetilde{k}^2\overline{Z}\big)^2+mM\widetilde{k}^2\overline{Z}+m^2\right)\;; \tag{42}$$

in summary, we emphasize that to obtain Eqs. (37)–(42) we have contracted both sides of the first equation with $\widetilde{S}_\mu$ and expanded the diquark propagator *à la* Eq. (28).

With these expressions, one may proceed to compute the bare quark contribution to the proton spin using the set of parameters determined from fits to the proton electromagnetic form factors, given in Table I. Using these values in the conventional formalism of Sec. II B that led to Eq. (16), we found $a_0 = 0.784$ — a value which may also be recovered from the hyperspherical formalism as given by Eq. (41). Incidentally, this figure is in accord with the moment of the scalar diquark contribution to the quark helicity PDF obtained in a typical light-front quark model (see Eqs. (61) and (62) of Ref. [10]):

$$\Delta q_s \;=\; \frac{1}{3}\,(2\,\Delta u\;-\;\Delta d)\;\approx\;0.75\;; \tag{43}$$

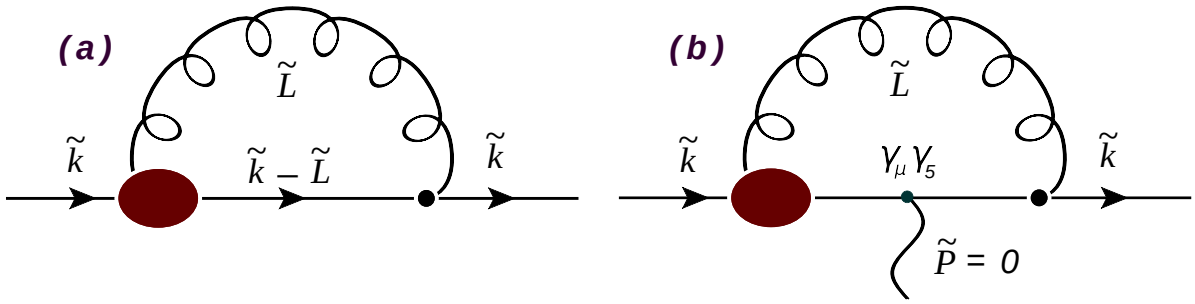

FIG. 4. (Color online) (**a**) The diagram leading to the DSE for a quark of momentum $\widetilde{k}$ dressed by a nonperturbative gluon carrying loop momentum $\widetilde{L}$. (**b**) The corresponding diagram for the quark axial-vector vertex BSE, responsible for the $\widetilde{k}$-dependent gluonic dressing correction to the axial charge of an individual quark. In the flavor-singlet channel, additional unquenching loop diagrams also contribute, as described in Ref. [55].

this latter expression assumed an $\mathbf{SU(2)} \otimes \mathbf{SU(2)}$ structure for the proton's spin-flavor wave function.

We point out as well that the axial-singlet EDF $\overline{a}_0(\widetilde{k}^2)$ given by Eq. (42) is not restricted to be positive-definite, unlike the analogous electromagnetic charge EDF $\overline{f}_1(\widetilde{k}^2)$ of Eq. (35), which is related to the zeroth moments of traditional probabilistic quark density functions. In fact, for certain parameter combinations, $\overline{a}_0(\widetilde{k}^2)$ may experience substantial negative downturns at larger spacelike quark momenta, $\widetilde{k} \geq 1$ GeV. However, for the set of fitting parameters that best describes proton form factor data, this effect is not evident, and the axial-singlet EDF $\overline{a}_0(\widetilde{k})$ is instead dominated by a soft peak centered roughly at $\widetilde{k} \lesssim 0.2$ GeV, as shown in Fig. 3 as the maroon-dashed line.

Owing mainly to the similarity of the explicit $\widetilde{k}^2$ dependence appearing in Eqs. (35) and (42), the shapes of these distributions closely track each other, with $f_1(\widetilde{k}^2) \approx \overline{a}_0(\widetilde{k}^2)$, particularly for $\widetilde{k}^2 \ll m^2$. Ultimately, we interpret this behavior as following from the common origin of both expressions in the diagrams of Fig. 1, which at $\widetilde{q} = 0$ differ only by the appearance of γ_5.

Moreover, for the higher $\sim\langle\widetilde{k}^2\rangle$ moment of the axial-singlet EDF, we obtain the value

$$M^1_{\bar{a}_0} \;=\; 0.08125 \text{ GeV}^2 \,, \tag{44}$$

implying the proton's distribution of axial-singlet charge is relatively softer than the charge distribution [Eq. (36)] in the bare model.

IV. GLUON DRESSING EFFECT

We now incorporate numerical estimates of the effect of dressing the quark-axial current vertex with gluon exchange, which in principle may be determined from DSE-BSE analyses. Here, the relevant diagrams are displayed in Fig. 4, wherein panel (**a**) illustrates the dressed propagator responsible for QCD's quark DSE, while panel (**b**) demonstrates the realization of the BSE for the quark-level coupling of the axial-vector current dressed by soft gluon exchange. Naturally, the infrared momenta at which this effect is of interest demands the use of nonperturbative methods, and the standard procedure requires a prescription-dependent truncation of the quark-gluon vertex (shown as the blobs in Fig. 4).

In the context of BSE analyses [15, 50–53], the dressed axial-vector vertex is represented by the structure $\Gamma^{fg}_{5\mu}(\widetilde{K};\widetilde{P})$, which is understood to connect an incoming quark of flavor g and momentum $\widetilde{K}_- = \widetilde{K} - (1-\eta)\widetilde{P}$ to an outgoing quark of flavor f and momentum $\widetilde{K}_+ = \widetilde{K} + \eta\widetilde{P}$; here $\widetilde{P}$ and $\widetilde{K}$ represent the total and relative momentum of the quark pair, and η is a dimensionless parameter upon which calculations cannot depend. Thus, for our purposes, we require the case $\widetilde{P} = 0$, such that $\widetilde{K}_+ = \widetilde{K}_- = \widetilde{K} \equiv \widetilde{k}$, and we take the diagonal isospin-independent vertex $f = g$, as described in Ref. [53]. Then the structure of the quark-axial vector vertex of relevance here is simply

$$\overline{u}(\widetilde{k})\ \Gamma_{5\mu}(\widetilde{k};0)\ u(\widetilde{k}) \ = \ \overline{u}(\widetilde{k})\ \gamma_5 \left[\gamma_\mu F_R(\widetilde{k};0) + \ldots\right]\ u(\widetilde{k})\ , \tag{45}$$

and the ellipsis in Eq. (45) above represents additional components of the vertex that do not contribute in the present analysis.

We therefore make the identification $f_g(\widetilde{k}) \equiv F_R(\widetilde{k};0)$ mentioned in Sec. III A, and directly insert the numerical results reported in Ref. [53] to smear the bare model axial charge as in Eq. (24). We also note that Ref. [53] was aimed at the quark's isovector axial vertex, and therefore neglected the "unquenching" effect of higher-order quark loops within the dressing diagram of Fig. 4(**b**), as such corrections are charge-independent and thus cancel for nonsinglet combinations. Unquenching effects do in principle contribute to the axial-singlet matrix element, however, and have been considered in Refs. [54, 55]. We assess the potential impact of this additional physics below.

The behavior of $f_g(\widetilde{k})$ depends crucially on the truncation scheme used to obtain the effective quark-gluon vertices in the panels of Fig. 4. To get a sense for this source of prescription dependence within the quenched calculation, we compute the correction following

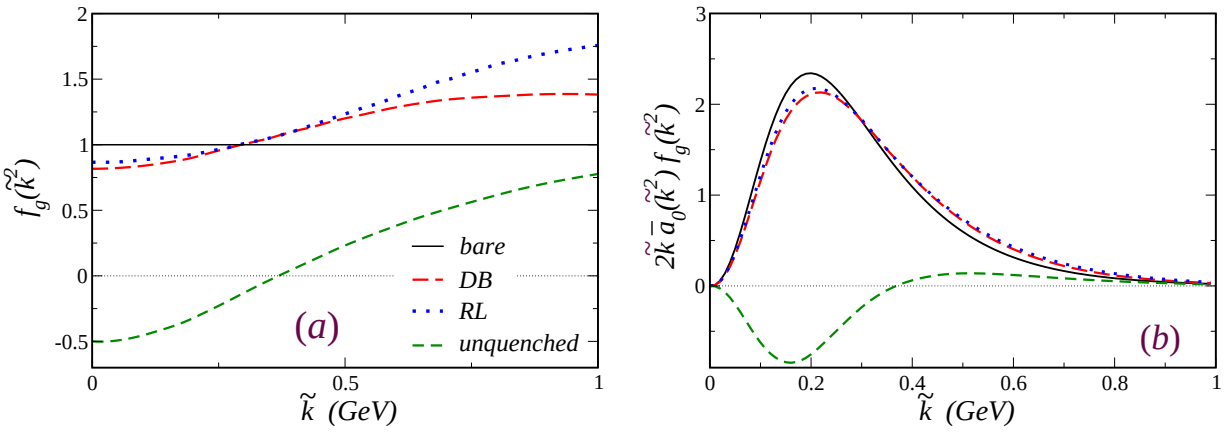

FIG. 5. (Color online) (**a**) The gluon dressing function $f_g(\widetilde{k}^2)$ under several different scenarios: the perturbative limit, $f_g(\widetilde{k}^2) = 1$ (solid black); using an improved dynamical chiral symmetry-breaking kernel in the quenched BSE, $f_g^{\rm DB}(\widetilde{k}^2)$ (red-dashed); with the quenched rainbow-ladder truncation method $f_g^{\rm RL}(\widetilde{k}^2)$ (blue-dotted); and using the result of a calculation [55] that included the effects of unquenching which contribute to the axial-singlet charge (green-short-dashed). (**b**) A plot of the integrand of Eq. (24) $2\widetilde{k}\,\overline{a}_0(\widetilde{k}^2)\,f_g(\widetilde{k}^2)$, taking for $f_g(\widetilde{k}^2)$ the gluon dressing functions shown in panel (**a**), retaining the aforementioned linestyles.

from both schemes treated in Ref. [53] — the rainbow-ladder scheme (RL), and an ansatz based on a specific realization of dynamical symmetry breaking (DB), which we take numerically from Fig. 1 of Ref. [53]. Referring to these as $f_g^{\rm RL}(\widetilde{k})$ (blue-dotted) and $f_g^{\rm DB}(\widetilde{k})$ (red-dashed), we plot both dressing functions against $\widetilde{k}$ in Fig. 5(**a**). Plainly, both truncation schemes predict a suppression of the quark's axial charge for the lowest infrared momenta $\widetilde{k} \lesssim 0.3$ GeV, but substantial enhancements beyond — particularly for the RL prescription, which overhangs the DB scheme by $\sim$25% for $\widetilde{k} \sim 1$ GeV. Having determined the axial EDF of Eq. (42) we may fold these extractions for the quenched gluon dressing function into Eq. (24) to determine the overall effect, plotting the integrands responsible for a_0', $2\widetilde{k}\,f_g^{\rm RL}(\widetilde{k}^2)\,\overline{a}_0(\widetilde{k}^2)$ (blue-dotted) and $2\widetilde{k}\,f_g^{\rm DB}(\widetilde{k}^2)\,\overline{a}_0(\widetilde{k}^2)$ (red-dashed), in Fig. 5(**b**) alongside the bare or "undressed" scenario, $f_g(\widetilde{k}^2) = 1$ (black-solid).

From this, we find the net correction to the quark helicity contribution from quenched

gluon dressing to be

$$\left(\frac{a_0'}{a_0}\right) - 1 \;=\; -0.04\% \quad \text{(DB scheme)} \;, \tag{46}$$

$$\;=\; +2.98\% \quad \text{(RL scheme)} \;. \tag{47}$$

The magnitude of the effect from quenched gluon dressing is therefore quite small, and in the present analysis, actually consistent with zero in the sense that, depending upon the choice of truncation scheme, one may obtain a modest enhancement (RL) or tiny suppression (DB) of the proton's total quark helicity. The smallness of the effect can be understood from the momentum dependence shown in Fig. 5(**b**), in which the interplay of the shapes of $f_g(\widetilde{k}^2)$ and $\overline{a}_0(\widetilde{k}^2)$ are such that the axial-singlet charge is slightly suppressed at low $\widetilde{k}$ and enhanced at higher $\widetilde{k}$. These two effects largely cancel, however, in the integral over $\widetilde{k}$ involved in the computation of a_0' according to Eq. (24), such that $a_0' \approx a_0$, and we conclude the quenched dressing effect in a_0 to be minimal.

As pointed out above, while the diagram of Fig. 4(**b**) figures in the dressing of both isovector *and* isoscalar (*i.e.,* flavor singlet) axial-vector quark vertices, the latter can receive additional contributions from higher-order diagrams involving the coupling of the axial-vector current to virtual quark loops closely connected to axial anomaly triangle graphs shown, *e.g.,* in Fig. 12 of Ref. [55]. As is typical of unquenched nonperturbative calculations, obtaining a systematic treatment of the dynamical quark loop effect is challenging. There is a significant level of dependence on renormalization scales, and the calculation in Ref. [55] employed a two-flavor approximation.

In the end, this procedure leads to the unquenched dressing function $f_g^{\text{unq.}}(\widetilde{k}^2)$ plotted as the green-short-dashed curve in Fig. 5(**a**), with a very sharp suppression of the quark's axial-singlet charge at low $\widetilde{k}$, which even attains negative values for $\widetilde{k} \lesssim 0.4$ GeV. Including this unquenching effect as computed in Ref. [55] — again using Eq. (24) — we find a dramatic suppression of the nucleon's axial-singlet charge, which in fact becomes slightly negative:

$$a_0' \;=\; -0.111 \quad \text{(unquenched scheme)} \;, \tag{48}$$

a value representing -14% of the bare axial-singlet nucleon charge, and which corresponds to the integrand plotted as the green-short-dashed line in Fig. 5(**b**).

We therefore conclude unquenching virtual quark loop diagrams have the potential to suppress the nucleon's axial-singlet charge (and total quark helicity), despite the tiny size

of the corresponding effect from the quenched calculation.

V. CONCLUSION

In this paper we have proposed a model in Euclidean space formulated in terms of constituent quark degrees of freedom. The essential products of the resulting ECQM technology are density functions of the quark's Euclidean momentum (the EDFs) obtained from hyperspherical angular integrations of 4-dimensional amplitudes. The special value of these derived quantities is their ability to recover nucleon charges through integrals over the internal momenta of their constituent quarks, a fact that empowered us to couple them to predictions of other Euclidean analyses — in this case, BSEs.

Thus, having introduced this formalism, we tested it preliminarily by computing both the nucleon's quark charge density, as well as its axial-singlet charge. For the latter, this test assumed the form of an assessment of the impact of BSE calculations for the dressed quark axial-vector vertex. There are of course various sources of model dependence on the side of both our ECQM for the nucleon-quark interaction and of the BSE analyses. Despite these sources of model-dependence, we find the effect of the quenched gluon dressing to be small by itself — at most a several percent correction to the total quark helicity in the bare ECQM. In constrast, we find that unquenching quark loop contributions highly suppress the nucleon's quark helicity component, a point requiring further study.

Naturally, the analysis presented here is essentially exploratory, and if anything, suggests the need for further refinements. For instance, the scalar diquark picture alone cannot realistically approximate the nucleon's full spin structure as evidenced by the large value we obtain for the bare axial-singlet charge ($a_0 = 0.784$); a fuller calculation would therefore involve spin-1 diquark exchanges, which in general are necessary to obtain an authentic flavor decompostion of the nucleon helicity.

At the same time, it is reasonable to expect that the qualitative *shape* obtained for $\overline{a}_0(\widetilde{k})$ shown in Fig. 5 for the present scalar diquark ECQM would hold also for amplitudes involving spin-1 exchanges, so that the essential details of such a calculation would resemble our presentation here. That being the case, our ultimate conclusion is unlikely to change: models formulated with bare constituent quarks receive vanishing corrections to the total quark helicity from quenched gluon loops, but can experience huge suppressions of the quark spin

from higher-order unquenching diagrams. This finding places an increased premium upon elucidating the details of how the unquenched dressing effect enters the the spin decomposition of Eq. (1), and its interaction with the quark and gluon angular momenta contained therein.

Similarly, it should be noted that other possible considerations have not been treated systematically, including the momentum dependence of the constituent quark's dynamical mass, the implementation of which would require a self-consistent scheme not typical of the fitted constituent quark model presented here. Such issues, as well as continued improvements to the Euclidean hyperspherical formalism and BSEs for the axial-vertex dressing functions will be of enormous value in extending the current state-of-the-art regarding quark helicity, the nucleon spin problem, and Euclidean modeling of nucleon structure.

VI. ACKNOWLEDGEMENTS

We thank Ian Cloët, Javier Menéndez, Brian Tiburzi, André Walker-Loud, Nodoka Yamanaka, and Xilin Zhang for helpful exchanges. The work of TJH and GAM was supported by the U.S. Department of Energy Office of Science, Office of Basic Energy Sciences program under Award Number DE-FG02-97ER-41014. The work of MA was supported under NSF Grant No. 1516105.

Appendix A: Euclidean space conventions

We proceed using the Minkowski $\leftrightarrow$ Euclidean transcription dictionary as outlined in, *e.g.,* Refs. [17, 20], wherein 4-momenta and Dirac matrices transform according to

$$\begin{aligned} k^0 &= ik_4 \ , & k^j &= -k_j \ , \\ \gamma^0 &= \gamma_4 \ , & \gamma^j &= i\gamma_j \ ; & j &\in \{1,2,3\} \ . \end{aligned} \tag{A1}$$

The Dirac algebra in this setting is then specified by

$$\Big\{\gamma_\mu, \gamma_\nu\Big\} \ = \ 2\,\delta_{\mu\nu} \ , \tag{A2}$$

such that the Euclidean inner product for any two 4-vectors $\widetilde{a}_\mu\,, \widetilde{b}_\mu$ is

$$\widetilde{a}\cdot\widetilde{b} \ \equiv \ \sum_\mu \ \widetilde{a}_\mu \widetilde{b}_\mu \ = \ \widetilde{a}_1\,\widetilde{b}_1 + \cdots + \widetilde{a}_4\,\widetilde{b}_4 \ , \tag{A3}$$

and, by extension,

$$\widetilde{\not{p}} \;\equiv\; \gamma_1\,\widetilde{p}_1 + \cdots + \gamma_4\,\widetilde{p}_4 \;. \tag{A4}$$

We also note the definition

$$\gamma_5 \;=\; -\gamma_1\,\gamma_2\,\gamma_3\,\gamma_4 \;. \tag{A5}$$

We may give explicit expressions for the Euclidean Dirac spinors, which we obtain following the conventional Wick rotation as

$$u_\lambda(p) \;=\; \sqrt{M+p^0}\,\begin{pmatrix} \chi_\lambda \\ \frac{\sigma\cdot\mathbf{p}}{M+p^0}\,\chi_\lambda \end{pmatrix} \quad\rightarrow\quad u_\lambda(\widetilde{p}) \;=\; \sqrt{M+i\widetilde{p}_4}\,\begin{pmatrix} \chi_\lambda \\ \frac{-\sigma\cdot\widetilde{\mathbf{p}}}{M+i\widetilde{p}_4}\,\chi_\lambda \end{pmatrix} \;, \tag{A6}$$

where the helicity states $\chi_{[\lambda=\uparrow\downarrow]} = \begin{pmatrix} 1 \\ 0 \end{pmatrix}, \begin{pmatrix} 0 \\ 1 \end{pmatrix}$ are proportional to the standard eigenvectors of σ_3. These spinors are endowed with the typical normalization,

$$\overline{u}\,u \;=\; 2M, \qquad \overline{u}(\widetilde{p})\,\gamma_\mu\,u(\widetilde{p}) = 2i\,\widetilde{p}_\mu \;, \tag{A7}$$

and obey the Dirac Equation

$$\overline{u}(\widetilde{p}')(i\widetilde{\not{p}}' + M) = (i\widetilde{\not{p}} + M)u(\widetilde{p}) = 0 \;. \tag{A8}$$

Moreover, in Euclidean space, the Gordon Identity assumes the slightly altered form

$$\overline{u}(\widetilde{p}')\,\gamma_\mu\,u(\widetilde{p}) \;=\; \frac{1}{2M}\,\overline{u}(\widetilde{p}')\left\{-i\widetilde{P}_\mu \;+\; \sigma_{\mu\nu}\widetilde{q}_\nu\right\}u(\widetilde{p}) \;, \tag{A9}$$

where we have defined $\widetilde{P}_\mu \equiv \widetilde{p}'_\mu + \widetilde{p}_\mu$ and $\sigma_{\mu\nu} \equiv (i/2)[\gamma_\mu, \gamma_\nu]$. By similar logic, we obtain the general form for the extended electromagnetic vertex of the proton,

$$\overline{u}(\widetilde{p}')\,\Gamma_\mu\big(\widetilde{p}',\widetilde{p}\big)\,u(\widetilde{p}) \;=\; \overline{u}(\widetilde{p}')\left\{F_1(\widetilde{q}^2)\,\gamma_\mu \;+\; F_2(\widetilde{q}^2)\,\sigma_{\mu\nu}\frac{\widetilde{q}_\nu}{2M}\right\}u(\widetilde{p}) \;. \tag{A10}$$

Appendix B: Hyperspherical formalism

In the hyperspherical formalism [33–36], numerator algebra leads to covariant expressions involving inner products which we represent in terms of the Gegenbauer polynomials, of which only the lowest are relevant for the present analysis:

$$\begin{aligned} C_0(x) \;&=\; 1 \;, \qquad & C_1(x) \;&=\; 2x \;, \\ C_2(x) \;&=\; 4x^2 - 1 \;. \end{aligned} \tag{B1}$$

Hyperspherical integrals may be separated into radial and angular parts according to

$$\int d^d\widetilde{k} \;=\; \int d\widetilde{k}\; \widetilde{k}^{d-1} \int d\Omega_{\hat{k}}^{(d)} \;, \tag{B2}$$

and we of course take $d = 4$ in the integrations over $d\Omega_{\hat{k}} \equiv d\Omega_{\hat{k}}^{(4)}$ $\left(= \sin^2\psi \sin\theta \, d\phi \, d\theta \, d\psi\right)$ in Sec. III; these can then be carried out in practice using well-known orthogonality properties:

$$\int d\Omega_{\hat{b}} \; C_m\big(\hat{a}\cdot\hat{b}\big) \; C_n\big(\hat{b}\cdot\hat{c}\big) \;=\; \frac{2\pi^2\delta_{mn}}{n+1} \; C_n\big(\hat{a}\cdot\hat{c}\big) \;. \tag{B3}$$

These relations can be determined from an appropriate choice of hyperspherical coordinates, with a common selection [60] being

$$k_\mu \;=\; \sqrt{\widetilde{k}^2} \begin{pmatrix} \sin\psi \, \sin\theta \, \cos\phi \\ \sin\psi \, \sin\theta \, \sin\phi \\ \sin\psi \, \cos\theta \\ \cos\psi \end{pmatrix} \;. \tag{B4}$$

---

[1] S.-J. Chang and T.-M. Yan, Phys. Rev. **D7**, 1147 (1973).

[2] G. P. Lepage and S. J. Brodsky, Phys. Rev. **D22**, 2157 (1980).

[3] G. A. Miller, Prog. Part. Nucl. Phys. **45**, 83 (2000), arXiv:nucl-th/0002059 [nucl-th].

[4] S. J. Brodsky, D. S. Hwang, B.-Q. Ma, and I. Schmidt, Nucl. Phys. **B593**, 311 (2001), arXiv:hep-th/0003082 [hep-th].

[5] B. L. G. Bakker *et al.*, *Proceedings, International Conference on Light-Cone Physics: Hadronic and Particle Physics: New Delhi, India, December 10-15, 2012*, Nucl. Phys. Proc. Suppl. **251-252**, 165 (2014), arXiv:1309.6333 [hep-ph].

[6] S. J. Brodsky, H.-C. Pauli, and S. S. Pinsky, Phys. Rept. **301**, 299 (1998), arXiv:hep-ph/9705477 [hep-ph].

[7] F. Cardarelli, E. Pace, G. Salmè, and S. Simula, Phys. Lett. **B357**, 267 (1995), arXiv:nucl-th/9507037 [nucl-th].

[8] J. Carbonell, B. Desplanques, V. A. Karmanov, and J. F. Mathiot, Phys. Rept. **300**, 215 (1998), arXiv:nucl-th/9804029 [nucl-th].

[9] G. A. Miller, Phys. Rev. **C66**, 032201 (2002), arXiv:nucl-th/0207007 [nucl-th].

[10] I. C. Cloët and G. A. Miller, Phys. Rev. **C86**, 015208 (2012), arXiv:1204.4422 [nucl-th].

[11] K. G. Wilson, Phys. Rev. **D10**, 2445 (1974).

[12] S. Aoki *et al.*, (2016), arXiv:1607.00299 [hep-lat].

[13] E. E. Salpeter and H. A. Bethe, Phys. Rev. **84**, 1232 (1951).

[14] Y. Nambu and G. Jona-Lasinio, Phys. Rev. **122**, 345 (1961).

[15] P. Maris and C. D. Roberts, Phys. Rev. **C56**, 3369 (1997), arXiv:nucl-th/9708029 [nucl-th].

[16] P. Maris and C. D. Roberts, Int. J. Mod. Phys. **E12**, 297 (2003), arXiv:nucl-th/0301049 [nucl-th].

[17] C. D. Roberts and A. G. Williams, Prog. Part. Nucl. Phys. **33**, 477 (1994), arXiv:hep-ph/9403224 [hep-ph].

[18] G. Eichmann, *Hadron Properties from QCD Bound-State Equations*, Ph.D. thesis, Graz U. (2009), arXiv:0909.0703 [hep-ph].

[19] G. Eichmann and C. S. Fischer, Eur. Phys. J. **A48**, 9 (2012), arXiv:1111.2614 [hep-ph].

[20] I. C. Cloët and C. D. Roberts, Prog. Part. Nucl. Phys. **77**, 1 (2014), arXiv:1310.2651 [nucl-th].

[21] H. Meyer and P. J. Mulders, Nucl. Phys. **A528**, 589 (1991).

[22] P. J. Mulders, A. W. Schreiber, and H. Meyer, Nucl. Phys. **A549**, 498 (1992).

[23] R. Jakob, P. J. Mulders, and J. Rodrigues, Nucl. Phys. **A626**, 937 (1997), arXiv:hep-ph/9704335 [hep-ph].

[24] F. Gross, G. Ramalho, and M. T. Peña, Phys. Rev. **D85**, 093006 (2012), arXiv:1201.6337 [hep-ph].

[25] B. C. Tiburzi and G. A. Miller, Phys. Rev. **D67**, 054014 (2003), arXiv:hep-ph/0210304 [hep-ph].

[26] G. A. Miller and B. C. Tiburzi, Phys. Rev. **C81**, 035201 (2010), arXiv:0911.3691 [nucl-th].

[27] M. Diehl, Phys. Rept. **388**, 41 (2003), arXiv:hep-ph/0307382 [hep-ph].

[28] A. V. Belitsky and A. V. Radyushkin, Phys. Rept. **418**, 1 (2005), arXiv:hep-ph/0504030 [hep-ph].

[29] J. O. Gonzalez-Hernandez, S. Liuti, G. R. Goldstein, and K. Kathuria, Phys. Rev. **C88**, 065206 (2013), arXiv:1206.1876 [hep-ph].

[30] T. J. Hobbs, M. Alberg, and G. A. Miller, Phys. Rev. **C91**, 035205 (2015), arXiv:1412.4871 [nucl-th].

[31] M. Burkardt, M. R. Frank, and K. L. Mitchell, Phys. Rev. Lett. **78**, 3059 (1997), arXiv:hep-ph/9611256 [hep-ph].

[32] L. Chang, I. C. Cloët, J. J. Cobos-Martinez, C. D. Roberts, S. M. Schmidt, and P. C. Tandy, Phys. Rev. Lett. **110**, 132001 (2013), arXiv:1301.0324 [nucl-th].

[33] T. Blum, Phys. Rev. Lett. **91**, 052001 (2003), arXiv:hep-lat/0212018 [hep-lat].

[34] M. J. Levine and R. Roskies, Phys. Rev. **D9**, 421 (1974).

[35] R. Z. Roskies, M. J. Levine, and E. Remiddi, Adv. Ser. Direct. High Energy Phys. **7**, 162 (1990).

[36] J. L. Rosner, Annals Phys. **44**, 11 (1967).

[37] J. Ashman *et al.* (European Muon), *Internal spin structure of the nucleon. Proceedings, Symposium, SMC Meeting, New Haven, USA, January 5-6, 1994*, Phys. Lett. **B206**, 364 (1988).

[38] J. Ashman *et al.* (European Muon), *Internal spin structure of the nucleon. Proceedings, Symposium, SMC Meeting, New Haven, USA, January 5-6, 1994*, Nucl. Phys. **B328**, 1 (1989).

[39] F. Myhrer and A. W. Thomas, Phys. Rev. **D38**, 1633 (1988).

[40] F. Myhrer and A. W. Thomas, Phys. Lett. **B663**, 302 (2008), arXiv:0709.4067 [hep-ph].

[41] A. W. Thomas, Phys. Rev. Lett. **101**, 102003 (2008), arXiv:0803.2775 [hep-ph].

[42] R. L. Jaffe, Phys. Lett. **B365**, 359 (1996), arXiv:hep-ph/9509279 [hep-ph].

[43] X.-D. Ji, Phys. Rev. Lett. **78**, 610 (1997), arXiv:hep-ph/9603249 [hep-ph].

[44] B. W. Filippone and X.-D. Ji, Adv. Nucl. Phys. **26**, 1 (2001), arXiv:hep-ph/0101224 [hep-ph].

[45] J. Blümlein and H. Böttcher, Nucl. Phys. **B636**, 225 (2002), arXiv:hep-ph/0203155 [hep-ph].

[46] E. Leader, A. V. Sidorov, and D. B. Stamenov, Phys. Rev. **D73**, 034023 (2006), arXiv:hep-ph/0512114 [hep-ph].

[47] M. Hirai, S. Kumano, and N. Saito, Phys. Rev. **D74**, 014015 (2006), arXiv:hep-ph/0603213 [hep-ph].

[48] D. de Florian, G. A. Navarro, and R. Sassot, Phys. Rev. **D71**, 094018 (2005), arXiv:hep-ph/0504155 [hep-ph].

[49] A. J. Chambers *et al.*, Phys. Rev. **D92**, 114517 (2015), arXiv:1508.06856 [hep-lat].

[50] P. Maris, C. D. Roberts, and P. C. Tandy, Phys. Lett. **B420**, 267 (1998), arXiv:nucl-th/9707003 [nucl-th].

[51] M. Bhagwat, M. A. Pichowsky, and P. C. Tandy, Phys. Rev. **D67**, 054019 (2003), arXiv:hep-ph/0212276 [hep-ph].

[52] M. S. Bhagwat, L. Chang, Y.-X. Liu, C. D. Roberts, and P. C. Tandy, Phys. Rev. **C76**, 045203 (2007), arXiv:0708.1118 [nucl-th].

[53] L. Chang, C. D. Roberts, and S. M. Schmidt, Phys. Rev. **C87**, 015203 (2013),

arXiv:1207.5300 [nucl-th].

[54] N. Yamanaka, T. M. Doi, S. Imai, and H. Suganuma, Phys. Rev. **D88**, 074036 (2013), arXiv:1307.4208 [hep-ph].

[55] N. Yamanaka, S. Imai, T. M. Doi, and H. Suganuma, Phys. Rev. **D89**, 074017 (2014), arXiv:1401.2852 [hep-ph].

[56] V. R. Zoller, Z. Phys. **C53**, 443 (1992).

[57] W. Melnitchouk, A. W. Schreiber, and A. W. Thomas, Phys. Rev. **D49**, 1183 (1994), arXiv:nucl-th/9311008 [nucl-th].

[58] W. Melnitchouk and M. Malheiro, Phys. Rev. **C55**, 431 (1997), arXiv:hep-ph/9610331 [hep-ph].

[59] A. Bodek and J. L. Ritchie, Phys. Rev. **D23**, 1070 (1981).

[60] M. E. Peskin and D. V. Schroeder, *An Introduction to quantum field theory* (1995).

[61] G. A. Miller, Phys. Rev. **C80**, 045210 (2009), arXiv:0908.1535 [nucl-th].

[62] J. J. Kelly, Phys. Rev. **C70**, 068202 (2004).

[63] J. Arrington, C. D. Roberts, and J. M. Zanotti, J. Phys. **G34**, S23 (2007), arXiv:nucl-th/0611050 [nucl-th].

[64] C. F. Perdrisat, V. Punjabi, and M. Vanderhaeghen, Prog. Part. Nucl. Phys. **59**, 694 (2007), arXiv:hep-ph/0612014 [hep-ph].

[65] J. Segovia, C. D. Roberts, and S. M. Schmidt, Phys. Lett. **B750**, 100 (2015), arXiv:1506.05112 [nucl-th].

[66] H. Li, P. Wang, D. B. Leinweber, and A. W. Thomas, Phys. Rev. **C93**, 045203 (2016), arXiv:1512.02354 [hep-ph].

[67] R. P. Feynman, M. Kislinger, and F. Ravndal, Phys. Rev. **D3**, 2706 (1971).

[68] P. J. Mohr, D. B. Newell, and B. N. Taylor, (2015), arXiv:1507.07956.